JOURNAL OF SOLID STATE CHEMISTRY **132,** 308–314 (1997)
ARTICLE NO. SC977464

New Mixed Valent Ferrites $(Tl_{1.5}Hg_{0.5})Sr_{3-x}Ba_xFe_2O_{9-\delta}$ $(0 \leq x \leq 2)$ with the Tl-2212-Type Structure

N. Nguyen, D. Groult,[1] P. Boullay, C. Michel, and B. Raveau

Laboratoire CRISMAT, CNRS–URA 1318, ISMRA, Universite de Caen, 14050 Caen Cedex, France

Received January 29, 1997; accepted May 1, 1997

A new series of layered ferrites $(Tl_{1.5}Hg_{0.5})Sr_{3-x}Ba_xFe_2O_{9-\delta}$ has been synthesized and characterized for the composition range $0 \leq x \leq 2$. The structure has been refined from powder XRD data and shown to be similar to that of the tetragonal Tl-2212-type superconducting copper oxides. Electron diffraction and high-resolution electron microscopy studies reveal a regular stacking of the [(Tl, Hg)O], [(Sr, Ba)O] and [FeO_2] layers without defects or atomic ordering on both the (Tl, Hg) and (Sr, Ba) sites. Magnetic susceptibility measurements and ^{57}Fe-Mössbauer spectroscopy have been performed for $(Tl_{1.5}Hg_{0.5})Sr_2BaFe_2O_{9-\delta}$. They provide evidence for antiferromagnetic ordering below 50 K with localized Fe^{3+} and Fe^{4+} species at 4.2 K, while intermediate valence states due to electron delocalization between iron sites must be taken into account at 293 K. The role of mercury is discussed.

INTRODUCTION

Recent studies of intergrowth phenomena in iron oxides have shown their great similarity with high T_c superconducting layered cuprates (1–7). The existence of a higher oxidation state for iron (FeIV/FeIII) compared to copper (CuIII/CuII) allows additional oxygen to be introduced into the structure so that the pyramidal copper layers are replaced by octahedral iron layers. It is thus the case for the Tl-1212- and Bi-2212-types ferrites $TlSr_3Fe_2O_8$ and $Bi_2Sr_3Fe_2O_9$ (8–10) whose structures are directly derived from those of the cuprates $TlSr_2CaCu_2O_8$ and $Bi_2Sr_2CaCu_2O_8$, respectively. Despite the fact that the Tl-2212 cuprate $Tl_2Ba_2CaCu_2O_8$ (11) which involves [TlO] bilayers can easily be synthesized, all attempts to prepare the iron counterpart failed. Based on results recently reported for the thallium–strontium-based cuprate $(Tl_{1.5}Hg_{0.5})Sr_{2.2}Ca_{0.8}Cu_2O_{8-\delta}$ (12), a new route for the synthesis of a 2212-type ferrite has been considered. Clearly, the partial substitution of mercury for thallium seems to stabilize the 2212 structure in those systems.

[1] To whom correspondence should be addressed.

The present paper deals with the preparation, structure, and magnetic properties of a new series of 2212-Tl-based ferrites $(Tl_{1.5}Hg_{0.5})Sr_{3-x}Ba_xFe_2O_{9-\delta}$ with a composition range $0 \leq x \leq 2$. The electronic configuration of iron is more specially investigated using ^{57}Fe Mössbauer spectroscopy as a local probe.

EXPERIMENTAL

Synthesis of the title compounds has been carried out in evacuated silica tubes using a two-step procedure. First, the oxide and carbonates Fe_2O_3, $SrCO_3$, and $BaCO_3$ were weighed in appropriate amounts, crushed in agate mortar, and heated at 1000°C for 24 h in an alumina crucible. Second, the mixture was intimately ground with the oxides Tl_2O_3, HgO, and SrO_2. The strontium dioxide was added in order to make the total stoichiometry of oxygen atoms equal to 9 atoms per formula unit. The powder was pressed as bars under a pressure of 1 t/cm^2 and the samples were put in alumina tubes and sealed in evacuated silica ampoules to prevent the high volatility of Tl_2O_3 and HgO above 600°C. The silica tubes were then slowly heated up to 800°C, held at this temperature for 12 h and cooled down to room temperature in 16 h.

X-ray diffraction data were collected by means of a Seifert vertical diffractometer equipped with a primary monochromator (Cu$K\alpha_1$ radiation) in the angular range $6° \leq 2\theta \leq 120°$ by step scanning with an increment of 0.02°. Lattice constants and structure were refined using the Rietveld analysis method (FULLPROF program (13)). The electron diffraction study was carried out on a Jeol 200CX electron microscope fitted with an eucentric goniometer ($\pm 60°$). High-resolution electron microscopy (HREM) was performed using a Topcon 002B microscope operating at 200 kV.

Magnetic measurements were carried out by means of SQUID magnetometer with an applied field of 3 kG in the temperature range 4.2–300 K and with a Faraday balance between 77 and 700 K. The Mössbauer spectra were recorded with a conventional constant acceleration

0022-4596/97 $25.00

spectrometer and a ^{57}Co:Rh source. The spectra were fitted using the MOSFIT program [14].

RESULTS AND DISCUSSION

For the above experimental conditions, a single-phase $(Tl_{1.5}Hg_{0.5})Sr_{3-x}Ba_xFe_2O_{9-\delta}$ is obtained for $0 \leq x \leq 2$. The electron diffraction investigation performed for $(Tl_{1.5}Hg_{0.5})Sr_2BaFe_2O_{9-\delta}$ evidences a tetragonal cell with $a \sim 3.84$ Å, $c \sim 30.1$ Å (Fig. 1). The conditions limiting the reflections (hkl): $h + k + l = 2n$ involve a I-type lattice like that found for the Tl-2212 cuprate $Tl_2Ba_2CaCu_2O_8$ (11) which exhibits indeed very similar XRD and ED patterns.

On the other hand, compared to its Bi-2212 counterpart $Bi_2Sr_3Fe_2O_9$ which has been more specially investigated (9, 10), neither superstructure reflections nor diffuse streaks indicative of commensurate or incommensurate modulation phenomena are observed here (Fig. 1). As can be seen in Table 1 the cell parameters refined from the XRD patterns increase continuously in the homogeneity range $0 \leq x \leq 2$ in agreement with the larger size of Ba^{2+} compared to Sr^{2+}.

The HREM investigation of $(Tl_{1.5}Hg_{0.5})Sr_2BaFe_2O_{9-\delta}$ microcrystals allowed the layer stacking to be checked. Typical overall [010] images are given in Fig. 2. They show that the stacking of the layers along the c axis is perfectly ensured throughout the whole crystal without any defect.

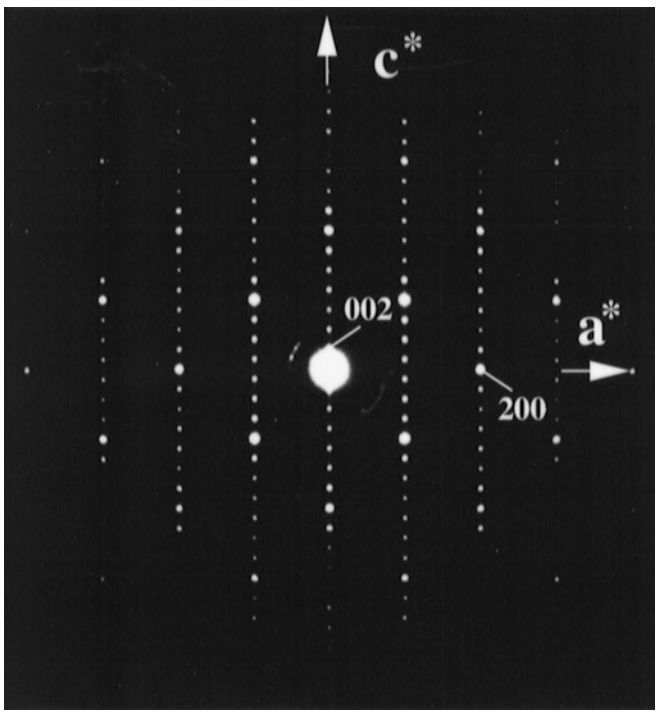

FIG. 1. (010) ED pattern of $(Tl_{1.5}Hg_{0.5})Sr_2BaFe_2O_{9-\delta}$ showing the tetragonal I-centred symmetry.

TABLE 1
Lattice Parameters Refined for the Series $(Tl_{1.5}Hg_{0.5})Sr_{3-x}Ba_xFe_2O_{9-\delta}$ from Powder XRD Patterns

x	a(Å) ± 0.0001	c(Å) ± 0.001	V(Å)^3 ± 0.05
0	3.8230	29.868	436.53
0.5	3.8330	29.950	440.02
1	3.8445	30.098	444.85
1.5	3.8661	30.418	454.65
2	3.8773	30.573	459.62

The enlarged image of Fig. 2b corresponds to a focus value close to -220 Å, where the low electron density zones are highlighted. The four rows of very bright staggered dots are correlated to the four $[AO]$ layers of a 2212 structure according to the sequence [(Ba, Sr)O]–[(Tl, Hg)O]–[(Tl, Hg)O]–[(Ba, Sr)O]. The three following rows of bright dots correspond to the oxygen atoms of the perovskite-type slice according to the sequence $[FeO_2]$–[(Ba, Sr)O]–$[FeO_2]$ as schematically drawn in Fig. 3. Note that no sign of Tl/Hg and Ba/Sr orderings can be detected from the HREM images, an even contrast is systematically observed. The interpretation is in good agreement with the theoretical image (Fig. 2b) calculated from the atomic positions refined from powder XRD data.

Taking into account of the regularity of the layer stacking, structure calculations have been performed for $(Tl_{1.5}Hg_{0.5})Sr_2BaFe_2O_{9-\delta}$ in the space group $I4/mmm$ starting with a structural model based on that of the Tl-2212 superconductor $Tl_2Ba_2CaCu_2O_8$. All the possible reflections allowed by the space group in the angular range used for this study (101 hkl for $10^\circ \leq 2\theta \leq 100^\circ$) were considered for the refinement. No distinction was made between Tl and Hg because of their similar scattering factors. The positions of the cations and of the oxygen atoms and finally the thermal factors of the heavy atoms were refined successively. The B factors of the oxygen atoms were arbitrarily fixed to 1 Å^2. However, because of the existence of some weak extra lines in the angular range $20^\circ \leq 2\theta \leq 40^\circ$, the introduction of HgO and of $BaCO_3$ as impurity phases has been considered in the refinement.

The refinement converged rapidly but with an intensity agreement factor which remains relatively high $R_I \sim 10\%$. Taking into account of previous results reported for Tl-based cuprates, the possibility of both static displacements and vacancies in the [(Tl, Hg)O] planes was assumed. A marked improvement of the fit was thus obtained when the oxygen O(3) was statistically distributed in 16(n) sites and when the occupancies of the Tl or Hg and O(3) sites were refined. The results are listed in Table 2 together with the profile and intensity R factors. The profile fit and the difference plot are shown in Fig. 4. Observe that in spite of the

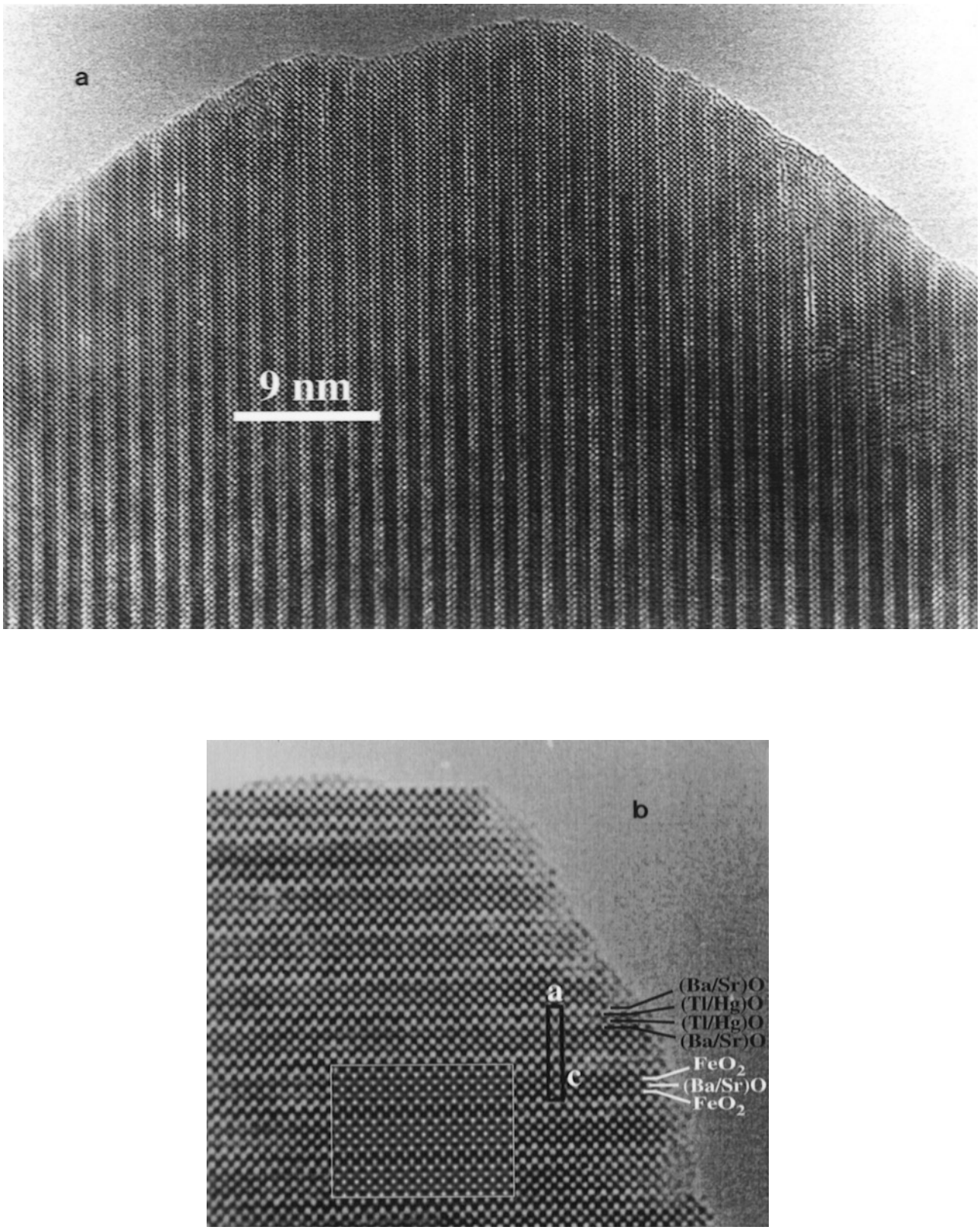

FIG. 2. (a) HREM image of $(Tl_{1.5}Hg_{0.5})Sr_2BaFe_2O_{9-\delta}$ along the [010] zone axis where the 2212 layer stacking is evidenced over a large area (b) Enlarged image with the calculated one corresponding to a crystal thickness of 12 Å and a focus value of -220 Å. The nature of the layers is indicated on the right part of the micrograph.

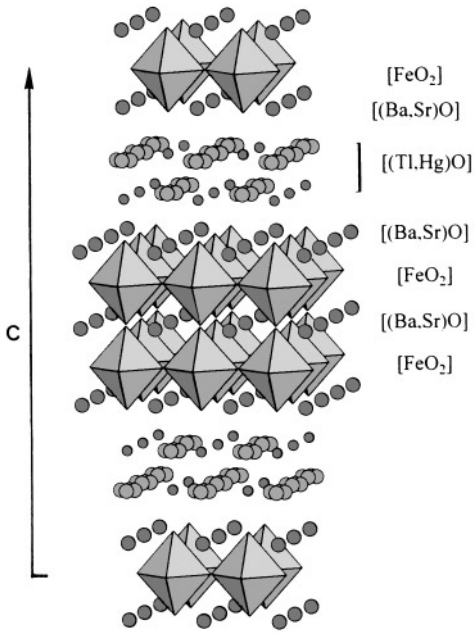

FIG. 3. Schematic drawing of the 2212-type structure for the series $(Tl_{1.5}Hg_{0.5})Sr_{3-x}Ba_xFe_2O_{9-\delta}$ $(0 \le x \le 2)$.

poor accuracy in the determination of the oxygen amount, it appears that the [(Tl, Hg)O] planes are likely oxygen deficient which is an usual feature for mercury-based cuprates. The selected metal–oxygen distances grouped in Table 3 are in good agreement with values previously reported for Tl-based related cuprates and ferrites (3–6). More specially, the

TABLE 2
Refined Variable Parameters for Nominal $(Tl_{1.5}Hg_{0.5})Sr_2BaFe_2O_{9-\delta}$ with e.s.d's in Parentheses

Atoms	Site	x	y	z	B (Å^2)	n
Tl,Hg	4*e*	0.0	0.0	0.2862(1)	0.3(1)	3.74(6)
Ba1/Sr1	4*e*	0.0	0.0	0.1300(2)	1.1(2)	1.20(4)/2.80(4)
Ba2/Sr2	2*a*	0.0	0.0	0.0	0.7(1)	0.80(4)/1.20(4)
Fe	4*e*	0.0	0.0	0.4360(3)	0.1(3)	4
O1	2*b*	0.0	0.0	0.5	1.0	2
O2	4*e*	0.0	0.0	0.354(1)	1.0	4
O3	16*n*	0.11(2)	0.0	0.221(2)	1.0	3.5(2)
O4	8*g*	0.0	0.5	0.4277(7)	1.0	8

Note. Space group: $I4/mmm$, $a = 3.8445(1)$ Å, $c = 30.098(1)$ Å. Thermal factors for oxygens were not refined. $R_p = 0.073$, $R_{wp} = 0.096$, $\chi^2 = 1.58$, $R_i = 0.074$.

interatomic Fe–O distances confirm the ability of iron to exhibit a strongly distorted octahedral coordination so that the structure can be described as built up from almost regular FeO_5 pyramids. Moreover, bond valence calculations based on the assumption of Brown and Altermat (15) yield $V_{Fe} = +3.23$ which supposes a mixed valence state between FeIII and FeIV in agreement with magnetic susceptibility measurements and ^{57}Fe-Mössbauer spectroscopy results.

The thermal variation of the magnetic susceptibility is reported in Fig. 5. At high temperature ($T > 400$ K) the linear variation of the inverse susceptibility characterizes a Curie–Weiss behavior with $\theta_p \sim -500$ K and $C_M \sim$

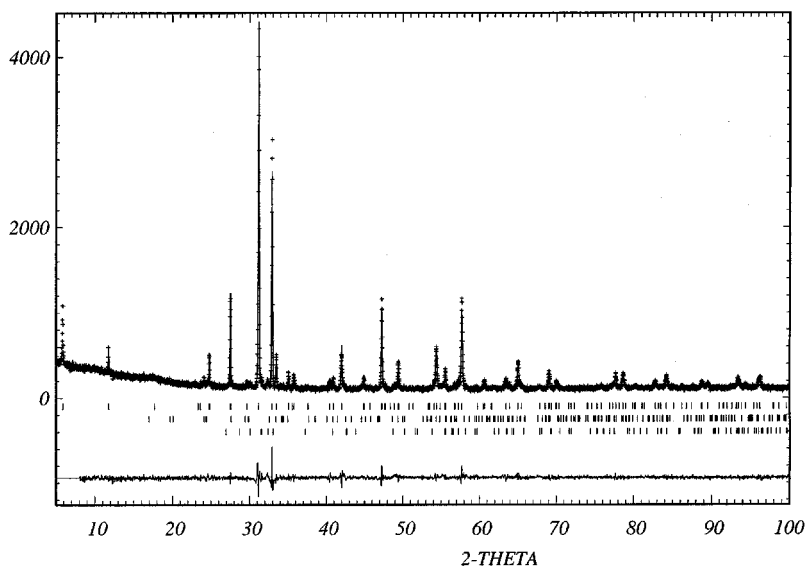

FIG. 4. X-ray powder diffraction diagrams: observed (crosses) calculated (solid) and Bragg angle positions (vertical bars) for the 2212 phase, $BaCO_3$, and HgO from top to bottom. The lower plot corresponds to the difference pattern.

TABLE 3
Selected Metal–Oxygen Distances with e.s.d's in Parentheses

M–O	Distance (Å)	*M*–O	Distance (Å)
Tl/Hg–O2[a]	2.06(4) × 1	Ba2/Sr2–O1	2.72(0) × 4
Tl/Hg–O3[a]	2.00(5) × 1	Ba2/Sr2–O4	2.90(2) × 8
Tl/Hg–O3[b]	2.45(4) × 2		
		Fe–O1[a]	1.93(1) × 1
Ba1/Sr1–O2	2.76(1) × 4	Fe–O2[a]	2.45(4) × 1
Ba1/Sr1–O3	2.78(5) × 1	Fe–O4[b]	1.939(3) × 4
Ba1/Sr1–O4	2.59(1) × 4		

[a] Distances along the *c* axis.
[b] Distances in the *ab* plane.

8.0 emu $Kmol^{-1}$. At low temperature an antiferromagnetic ordering is observed below 50 K which is confirmed by the Mössbauer spectroscopy data.

Figure 6 shows the ^{57}Fe-Mössbauer spectra of the powder sample $(Tl_{1.5}Hg_{0.5})Sr_2BaFe_2O_{9-\delta}$ at 4.2 and 293 K. Although it is not still completely established, a magnetic ordering is thus revealed at 4.2 K and the Mössbauer spectrum can be fitted as the sum of two main Zeeman sextets whose isomer shift (IS) and hyperfine field (Hf) values (Table 4) can be assigned to high spin Fe^{3+} and Fe^{4+} species. The relative intensities of the sites: $72 \pm 5\%$ for Fe^{3+} and $28 \pm 5\%$ for Fe^{4+}, lead for iron to a mean oxidation state of $+3.28$ in agreement with that deduced from bond valence calculations and magnetic susceptibility measurements. Note that the fit of the spectrum needs to take account of a third paramagnetic single line whose intensity less than 5% could be due to superparamagnetic small grains or to an impurity phase not visible on powder XRD patterns.

The Mössbauer spectrum recorded at 293 K (Fig. 6a) indicates the presence of pure electric quadrupolar interactions. It can be decomposed into two classical Lorentzian doublets (Table 4) whose isomer shifts of 0.23 and 0.10 mm/s respectively correspond to the typical variations which can be expected between 4.2 and 293 K for Fe^{3+} and Fe^{4+} species. However, it should be noted that at 293 K the

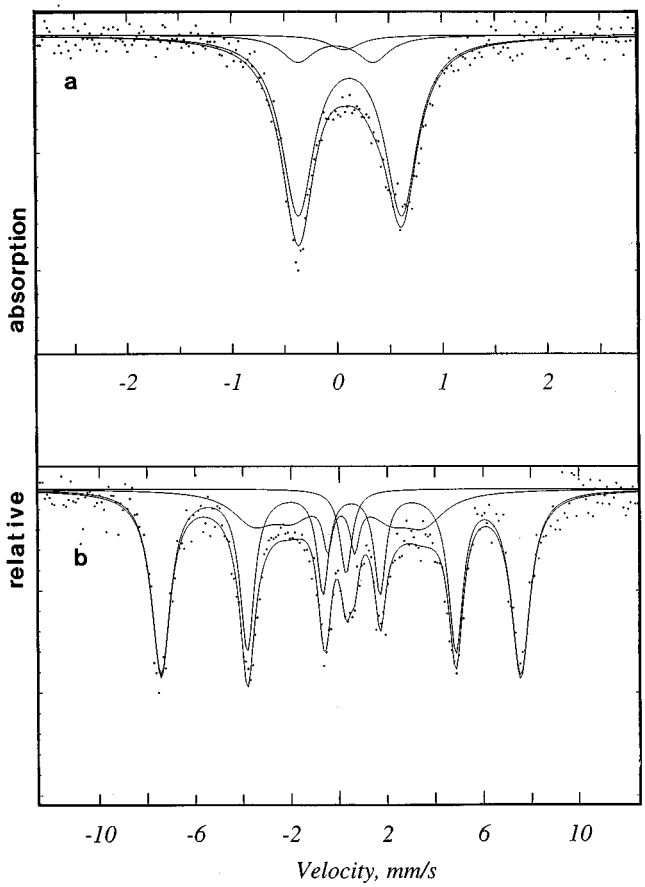

FIG. 6. Mössbauer resonance spectra of $(Tl_{1.5}Hg_{0.5})Sr_2BaFe_2O_{9-\delta}$ at (a) 293 and (b) 4.2 K.

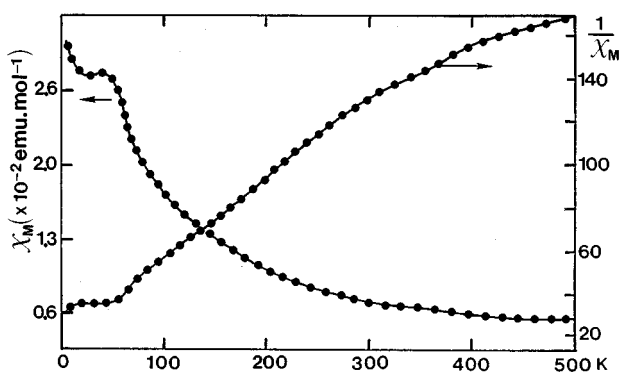

FIG. 5. Thermal dependence of the molar magnetic susceptibility of $(Tl_{1.5}Hg_{0.5})Sr_2BaFe_2O_{9-\delta}$.

TABLE 4
Fitted Values of the Hyperfine Mössbauer Parameters at 4.2 and 293 K for $(Tl_{1.5}Hg_{0.5})Sr_2BaFe_2O_{9-\delta}$

T (K)	Site	IS mm/s ± 0.01	2ε or QS mm/s ± 0.01	Hf Tesla ± 0.01	Intensity % ± 5
4.2	*A*	0.40	− 0.45	46.40	68
	B	0.15	− 0.11	21.90	27
	C[a]	0.40	0	—	5
293	*A*	0.23	0.98	—	84
	B	0.10	0.71	—	12
	C[a]	0.19	0	—	4

Note. IS, isomer shift relative to α-Fe; 2ε, quadrupole shift; QS, quadrupole splitting; Hf, hyperfine field.
[a] impurity phase.

intensity of the second site is roughly half of that observed at 4.2 K which suggests that an electron delocalization between iron sites takes place with increasing temperature as discussed for $TlSr_3Fe_2O_8$ and $TlSr_4Fe_2O_9$ (16).

Furthermore one can note that the isomer shift of the second site corresponds to a value which has been reported for the ferrites $SrFeO_{3-\delta}$ and $La_{1-x}Sr_xFeO_{3-\delta}$ (17–19). This has been explained on the basis of charge transfer phenomena which involve either disproportionation of Fe^{4+} into Fe^{3+} and Fe^{5+} or electron transfer of the type $Fe^{4+} + O^{2-} = Fe^{3+} + O^-$. According to Seguelong *et al.* (6) "such a charge transfer partially transforms Fe^{4+} into Fe^{3+} whose electronic configuration would be medium spin ($S = 3/2$) and whose isomer shift can be close to 0.10 mm/s at 293 K." This assumption also appears to be in agreement with the high distortion of the iron site (Table 3) which contributes to stabilize such an intermediate spin configuration as discussed elsewhere (20).

Let us now compare the Mössbauer spectrum collected at 293 K for this 2212 phase with that obtained for the 1212 type-oxide $TlSr_3Fe_2O_8$ (8). In this latter case, it has indeed been shown that three non-equivalent iron sites have to be considered to correctly fit the Mössbauer spectrum at 293 K, although only one iron crystallographic site was refined from XRD data. At a local scale, besides the possibility for iron to exhibit different charge states, it has been demonstrated from EFG calculations performed in the monopolar order for high spin Fe^{3+} that the existence of two Fe^{3+} sites with different values of the quadrupole splitting was due to local displacements along the *c* axis of the apical oxygen O(2). A similar situation has been more recently found for the Bi-based 2212 counterpart $Bi_{2+x}Sr_{3-x}Fe_2O_{9+\delta}$ (21) whose Mössbauer spectrum at 293 K has indeed been fitted using three classical Lorentzian doublets with isomer shifts close to 0.30 mm/s characteristic of high spin Fe^{3+} ($S = 5/2$). In that case, the existence of three Mössbauer sites has been explained on the basis of the structural investigation which implies a complex variation of the apical Fe–O(3) bond length due to the existence of an incommensurate modulation.

For $(Tl_{1.5}Hg_{0.5})Sr_2BaFe_2O_{9-\delta}$ the fact that only one Fe^{3+}-Mössbauer site has been observed can be explain on the basis of the peculiar behavior of the Hg^{2+} cations which are partially substituted for Tl^{3+} cations in order to stabilize the 2212-type structure. If one considers the numerous mercury-based superconductors which have been synthesized to date (22), it should be recalled that all the structures exhibit HgO_2 sticks aligned along the *c* axis. As a consequence of the stiffness of such HgO_2 sticks, no local displacements of the apical oxygen linked to Hg^{2+} can be expected.

This peculiar behavior led us to assume that for the 2212 ferrite the local oxygen environment of iron cannot be changed, hence implying one Fe^{3+}-Mössbauer site instead of two as observed for $TlSr_3Fe_2O_8$. Moreover, it should be pointed out that the quadrupole splitting values of the doublets (Table 4) are higher than those for $TlSr_3Fe_2O_8$ or $TlSr_4Fe_2O_9$ (16) which suggests that the symmetry of the local environment of iron is lower for the Tl-2212 phase than for the other two. Such a change appears in good agreement with the XRD data (Table 3) which shows that iron cations exhibit a pyramidal oxygen environment rather than a distorted octahedral one.

CONCLUSION

We have prepared a new series of Tl-2212-type ferrites $(Tl_{1.5}Hg_{0.5})Sr_{3-x}Ba_xFe_2O_{9-\delta}$ ($0 \leq x \leq 2$) which confirm the great ability of iron to adopt layered structures similar to that of the copper-based superconducting oxides.

In contrast to the Tl-1212 ($TlSr_3Fe_2O_8$)- and Tl-1201-0201 ($TlSr_4Fe_2O_9$)-type ferrites previously studied, the synthesis of the 2212 phases requires that 25% of the $5d^{10}$ Tl^{3+} cations are replaced by the isoelectronic Hg^{2+} cations in the double rock salt-type [TlO] planes.

^{57}Fe-Mössbauer spectroscopy data collected for the compound $(Tl_{1.5}Hg_{0.5})Sr_2BaFe_2O_{9-\delta}$ agree with the results deduced from magnetic measurements and Rietveld analysis. It is shown that at low temperature, iron exhibits localized species Fe^{3+} and Fe^{4+} leading to a mean oxidation state of $+3.28$ Å. At increasing temperature, an electronic delocalization between iron sites takes place leading to intermediate valence states.

ACKNOWLEDGMENT

The authors thank A. Maignan for carrying out the SQUID magnetic measurements.

REFERENCES

1. S. Lucas, D. Groult, N. Nguyen, C. Michel, M. Hervieu, and B. Raveau, *J. Solid State Chem.* **102,** 20 (1993).
2. V. Caignaert, P. Daniel, N. Nguyen, A. Ducouret, D. Groult, and B. Raveau, *J. Solid State Chem.* **112,** 126 (1994).
3. P. Daniel, L. Barbey, D. Groult, N. Nguyen, G. Van Tendeloo, and B. Raveau, *Eur. J. Solid State Inorg. Chem.* **31,** 235 (1994).
4. T. Fries, C. Steudtner, M. Schlichenmaier, S. Keimmler-Sack, T. Nissel, and R. P. Huebener, *J. Solid State Chem.* **108,** 8 (1994).
5. M. Hervieu, D. Pelloquin, C. Michel, M. T. Caldes, and B. Raveau, *J. Solid State Chem.* **118,** 227 (1995).
6. T. Seguelong, P. Maestro, J. C. Grenier, L. Fournes, and M. Pouchard, *Physica B* **215,** 427 (1995).
7. N. Nguyen, P. Daniel, D. Groult, B. Raveau, and J. M. Greneche, *Mater. Chem. Phys.* **45,** 33 (1996).
8. P. Daniel, L. Barbey, N. Nguyen, A. Ducouret, D. Groult, and B. Raveau, *J. Phys. Chem. Solids* **55,** 705 (1994).
9. Y. Lepage, W. R. McKinnon, J. M. Tarascon, and P. Barboux, *Phys. Rev. B* **40,** 6810 (1989).
10. O. Perez, H. Leligny, D. Grebille, P. Labbe, D. Groult, and B. Raveau, *J. Phys. Condens. Matter* **7,** 10003 (1995).

11. D. E. Cox, C. C. Torardi, M. A. Subramanian, J. Gopalakrishnan, and A. W. Sleight, *Phys. Rev. B* **38,** 6624 (1988).
12. A. Maignan, C. Martin, C. Michel, M. Hervieu, and B. Raveau, *Chem. Mater.* **7,** 1207 (1995).
13. J. Rodriguez-Carjaval, "FULLPROF: A Program for Rietveld Refinements and Pattern Matching Analysis," XVth Congress of Int. Union of Crystallography Toulouse, France, July 1990.
14. J. Teillet and F. Varret, unpublished Mosfit program.
15. D. Altermatt and I. D. Brown, *Acta Crystallogr. B* **41,** 240 (1985).
16. N. Nguyen, D. Groult, A. Ducouret, J. M. Greneche, and B. Raveau, *J. Phys. Condens. Matter* **8,** 6297 (1996).
17. M. Takano, J. Kawachi, N. Nakanish, and Y. Takeda, *J. Solid State Chem.* **39,** 75 (1981).
18. A. Wattiaux, L. Fournes, A. Demourgues, N. Bernaben, J. C. Grenier, and M. Pouchard, *Solid State Commun.* **77,** 489 (1991).
19. S. E. Dann, D. B. Currie, H. T. Weller, M. F. Thomas, and A. D. Al-Rawwas, *J. Solid State Chem.* **109,** 134 (1994).
20. B. Buffat, G. Demazeau, M. Pouchard, and P. Hagenmuller, *Proc. Indian Acad. Sci.* **93/3,** 313 (1984).
21. O. Perez, H. Leligny, D. Grebille, J. M. Greneche, P. Labbe, D. Groult, and B. Raveau, *Phys. Rev. B.* **55,** 1236 (1997).
22. B. Raveau, C. Michel, M. Hervieu, and A. Maignan, *J. Mater Chem.* **5,** 803 (1995).